

# Probing the Scalar Sector: Discovery Reach for Heavy Higgs Pairs at a $\sqrt{s} = 6$ TeV Muon Collider in the 2HDM Alignment Limit

Ijaz Ahmed,<sup>1,\*</sup> Muhammad Umar Farooq,<sup>2</sup> Farzana Ahmad,<sup>3,†</sup> and Jamil Muhammad<sup>4,‡</sup>

<sup>1</sup>*Federal Urdu University of Arts, Science and Technology, Islamabad, Pakistan*

<sup>2</sup>*Riphah International, Islamabad, Pakistan*

<sup>3</sup>*SERI, & College of Engineering, Konkuk University, Seoul 05029, South Korea*

<sup>4</sup>*Sang-Ho College & Department of Physics,*

*Konkuk University, Seoul 05029, South Korea*

(Dated: February 16, 2026)

## Abstract

This study provides a comprehensive phenomenological investigation into the discovery potential of heavy Higgs boson pairs ( $HH, HA, AA, H^+H^-$ ) at a  $\sqrt{s} = 6$  TeV Muon Collider. Utilizing the Two-Higgs-Doublet Model (2HDM) Type-I within the alignment limit ( $\sin(\beta - \alpha) \approx 1$ ), we evaluate two primary benchmarks with degenerate scalar masses of 1000 GeV (BP1) and 2000 GeV (BP2). Theoretical calculations performed reveal that Type-I branching fractions to third-generation fermions remain uniquely independent of  $\tan\beta$ , providing a stable signal across the investigated parameter space. We demonstrate that the Muon Collider environment allows for the precise identification of high-multiplicity hadronic final states. A key finding of this research is that the signal processes yield distinctive topological signatures: an 8-jet state ( $4j + 4b$ ) for charged pairs and a highly complex 12-jet state ( $8j + 4b$ ) for neutral pairs ( $HA/AA$ ). These signatures, combined with hard transverse momentum distributions and central pseudorapidity ( $|\eta| \leq 3$ ), allow for nearly absolute suppression of Standard Model backgrounds like  $t\bar{t}$ ,  $W^+W^-Z$ , and  $ZZZ$ . At an integrated luminosity of  $10 \text{ ab}^{-1}$ , we report a staggering statistical significance of 104,000 for the  $H^+H^-$  channel and 3343 for the  $HA$  channel in the BP1 scenario. Furthermore, total selection efficiencies were found to increase from approximately 20% at BP1 to 47% at BP2, suggesting that the decay products of heavier scalars are kinematically easier to resolve. We conclude that a 6 TeV Muon Collider offers an unparalleled discovery reach for the extended scalar sector, providing a definitive facility for probing physics beyond the Standard Model.

PACS numbers: 12.60.Fr, 14.80.Fd 12.60.Fr, 14.80.Ec, 13.66.Hk

Keywords: Muon Collider, 2HDM, Higgs Pair Production, BSM Phenomenology, Multi-TeV Physics.

---

\*Electronic address: [ijaz.ahmed@fuuast.edu.pk](mailto:ijaz.ahmed@fuuast.edu.pk)

†Electronic address: [farzana@konkuk.ac.kr](mailto:farzana@konkuk.ac.kr)

‡Electronic address: [mjamil@konkuk.ac.kr](mailto:mjamil@konkuk.ac.kr)

## I. INTRODUCTION

The discovery of the Higgs boson at the Large Hadron Collider (LHC) in 2012 [2, 3] provided the final piece of the Standard Model (SM), confirming the mechanism of spontaneous electroweak symmetry breaking (EWSB) and the origin of fundamental particle masses [4, 5]. Despite its success, the SM remains an incomplete description of the universe, failing to provide candidates for dark matter [25], account for the hierarchy problem [23, 30], or explain the observed matter-antimatter asymmetry. These deficiencies strongly suggest that the SM is an effective field theory valid up to an energy scale where new physics must emerge [24, 29]. Among the various proposed extensions, the Two-Higgs-Doublet Model (2HDM) stands as one of the most well-motivated and extensively studied extensions [6]. By introducing a second  $SU(2)_L$  scalar doublet, the model predicts a rich scalar sector consisting of five physical states: two CP-even bosons ( $h, H$ ), one CP-odd boson ( $A$ ), and a pair of charged Higgs bosons ( $H^\pm$ ) [7, 8]. Current experimental data from the LHC has constrained the scalar sector close to the “alignment limit,” where the coupling profile of the light CP-even scalar  $h$  becomes indistinguishable from that of the SM Higgs boson [9]. Consequently, searching for the heavier scalars ( $H, A, H^\pm$ ) and understanding their self-couplings is paramount for probing the structure of the extended scalar potential [10, 31].

While the LHC and the proposed High-Luminosity LHC (HL-LHC) will continue to refine Higgs measurements, their reach is often limited by large QCD backgrounds and low signal-to-background ratios in certain BSM channels [22]. Future lepton colliders offer a much cleaner experimental environment. Recently, the multi-TeV Muon Collider has emerged as a frontrunner for the next generation of high-energy physics facilities [11, 13, 32, 33]. Recently, the IMCC and US community have outlined a roadmap toward a 10 TeV facility [34, 45]. Since the muon is approximately 207 times more massive than the electron, synchrotron radiation is suppressed by a factor of  $(m_\mu/m_e)^4 \approx 10^9$ , allowing for circular acceleration to multi-TeV center-of-mass energies while maintaining high luminosity [12, 15]. A 6 TeV muon collider effectively combines the precision of  $e^+e^-$  machines with the high energy reach of hadron colliders, making it an ideal laboratory for probing heavy Higgs pair production [14, 16].

The production of Higgs boson pairs ( $HH, HA, AA, H^+H^-$ ) provides a direct probe into the scalar potential and the nature of the EWSB transition [26, 27]. In the 2HDM framework, these cross-sections can be significantly enhanced compared to the SM, potentially within the reach of a high-energy muon collider [28]. While this analysis focuses on the  $s$ -channel annihilation mechanism, which is highly effective at the  $\sqrt{s} = 6$  TeV scale, it is important to note that the

Vector Boson Fusion (VBF) contribution—as detailed by Han et al. (2021) [14] and Buttazzo et al. (2018) [27]—becomes increasingly significant at higher center-of-mass energies, eventually becoming the dominant production mode for heavy scalars in the multi-TeV regime [38, 44]. Accurate modeling of these processes requires sophisticated computational frameworks. Current analyses rely on automated tools such as `CalcHEP` [17] and `2HDMC` [18] for cross-section calculations, while event generation and kinematic analysis are typically performed via `MadGraph5_aMC@NLO` [19] and `MadAnalysis 5` [20], often supplemented by symbolic manipulators like `FeynHelpers` [21]. In this work, we perform a detailed phenomenological study of heavy Higgs pair production at a multi-TeV Muon Collider operating at  $\sqrt{s} = 6$  TeV. We evaluate the effective cross-sections and signal significance for the processes  $\mu^+\mu^- \rightarrow HH, HA, AA, H^+H^-$  within the 2HDM alignment limit. Our analysis considers two primary benchmark points (BP1 and BP2) corresponding to degenerate Higgs masses of 1000 GeV and 2000 GeV, respectively. By simulating both signal and relevant SM backgrounds ( $t\bar{t}$ ,  $W^+W^-Z$ ,  $ZZZ$ ) across integrated luminosities of  $3.6 \text{ ab}^{-1}$  and  $10 \text{ ab}^{-1}$ , we demonstrate the discovery potential of this facility for the BSM scalar sector.

## II. THEORETICAL FRAMEWORK

### A. 2HDM Types using `CalcHEP`

In this work, `CalcHEP` is utilized to calculate and distinguish the branching fractions of neutral and charged Higgs decays into various fermion pairs across the four types of the Two Higgs Doublet Model (2HDM). While the pair production rates are identical across all 2HDM types due to their dependence on gauge couplings, the branching fractions provide unique signatures as they depend on the specific Yukawa couplings of each model. As illustrated in Figure 1, the branching ratios for neutral Higgs decays ( $H/A \rightarrow b\bar{b}, t\bar{t}, \tau^+\tau^-$ ) at a mass scale of 2 TeV demonstrate that Type-I remains entirely independent of  $\tan\beta$ . In contrast, for  $\tan\beta > 5$ , the other models show distinct dominance: the  $H \rightarrow b\bar{b}$  decay mode is dominant in Type-II and IV, while the  $H \rightarrow t\bar{t}$  and  $H \rightarrow \tau^+\tau^-$  channels are significantly more prominent in Type-II and III compared to other configurations. The distinction between 2HDM types is further clarified through the analysis of the charged Higgs sector. As depicted in Figure 2, the branching fractions for  $H^+ \rightarrow t\bar{b}$  and  $H^+ \rightarrow \tau^+\nu_\tau$  exhibit a strong sensitivity to the  $\tan\beta$  parameter. While all 2HDM types exhibit similar behavior at low values ( $\tan\beta < 5$ ), they diverge significantly in the high  $\tan\beta$  region, allowing for the separation of Type-II and III from the others. Specifically, the  $H^+ \rightarrow t\bar{b}$  channel is

found to be the dominant decay mode in Type-I and IV, whereas the  $H^+ \rightarrow \tau^+ \nu_\tau$  mode becomes the presiding decay mechanism in Type-II and III. These variations highlight the potential for a multi-TeV muon collider to determine the specific type of the 2HDM through the measurement of these distinct fermionic decay signatures.

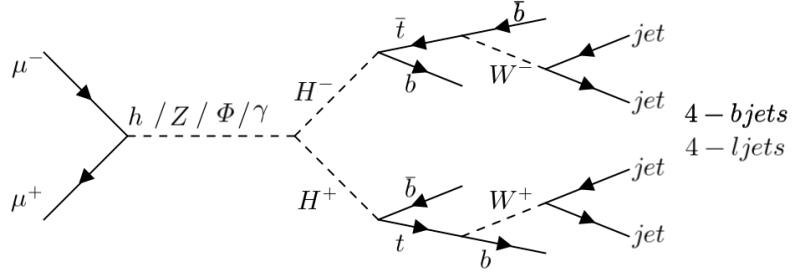


FIG. 1: Branching ratio vs  $\tan \beta$  for  $H/A \rightarrow b\bar{b}, t\bar{t}, \tau^+\tau^-$  at  $m_\phi = 2$  TeV.

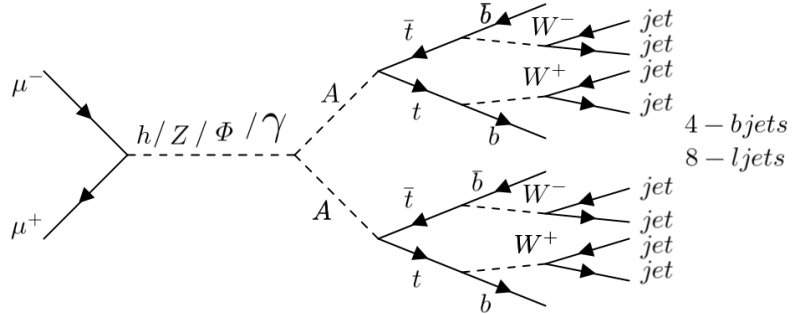


FIG. 2: Branching ratio vs  $\tan \beta$  for  $H^+ \rightarrow t\bar{b}$  and  $H^+ \rightarrow \tau^+ \nu_\tau$  at  $m_\phi = 2$  TeV.

## B. The Two-Higgs-Doublet Model (2HDM)

The 2HDM extends the SM by introducing a second complex scalar doublet. Both doublets  $\Phi_1$  and  $\Phi_2$  possess the same hypercharge  $Y = 1$  [6]. This extension results in five physical scalar states after EWSB:

- Two CP-even neutral scalars ( $h, H$ ), where  $h$  is typically identified as the 125 GeV SM-like Higgs.
- One CP-odd neutral scalar ( $A$ ).
- Two charged Higgs bosons ( $H^\pm$ ).

The scalar potential for a CP-conserving 2HDM with a softly broken  $Z_2$  symmetry is expressed as [6]:

$$\begin{aligned} V(\Phi_1, \Phi_2) = & m_{11}^2 \Phi_1^\dagger \Phi_1 + m_{22}^2 \Phi_2^\dagger \Phi_2 - [m_{12}^2 \Phi_1^\dagger \Phi_2 + \text{h.c.}] \\ & + \frac{1}{2} \lambda_1 (\Phi_1^\dagger \Phi_1)^2 + \frac{1}{2} \lambda_2 (\Phi_2^\dagger \Phi_2)^2 + \lambda_3 (\Phi_1^\dagger \Phi_1)(\Phi_2^\dagger \Phi_2) \\ & + \lambda_4 (\Phi_1^\dagger \Phi_2)(\Phi_2^\dagger \Phi_1) + \frac{1}{2} \lambda_5 [(\Phi_1^\dagger \Phi_2)^2 + \text{h.c.}] \end{aligned} \quad (1)$$

Two key parameters define the phenomenology of this model: the ratio of the two VEVs,  $\tan \beta = v_2/v_1$ , and the mixing angle  $\alpha$  between the neutral CP-even states [36]. In the “alignment limit,” defined by  $\sin(\beta - \alpha) \rightarrow 1$ , the properties of the light scalar  $h$  coincide with the SM Higgs boson [9]. Current global fits have significantly constrained the A2HDM parameter space [37]. To avoid Flavour Changing Neutral Currents (FCNC) at the tree level, discrete  $Z_2$  symmetries are imposed, leading to four distinct types of 2HDM summarized in Table II [10, 40].

### III. SIMULATION METHODOLOGY AND MUON COLLIDER SETUP

#### A. The Multi-TeV Muon Collider Environment

The Muon Collider represents a unique high-energy frontier facility that combines the advantages of both hadron and electron machines. Unlike protons, muons are fundamental particles, ensuring that the full center-of-mass energy ( $\sqrt{s}$ ) is available for the hard scattering process [11]. Furthermore, the power loss through synchrotron radiation for a particle of mass  $m$  and energy  $E$  scales as  $1/m^4$ . For a muon collider, this suppression relative to an electron machine is given by:

$$\frac{P_{\text{loss}}(\mu)}{P_{\text{loss}}(e)} = \left( \frac{m_e}{m_\mu} \right)^4 \approx 10^{-9} \quad (2)$$

This massive reduction in energy loss allows for circular acceleration to multi-TeV scales within a compact footprint [12]. Recent design challenges regarding siting at major labs like Fermilab have been addressed in the latest roadmap [42, 43].

#### B. Computational Framework and Event Generation

Numerical analysis is performed using a multi-stage simulation pipeline. Theoretical consistency—including vacuum stability and unitarity—is verified using `2HDMC 1.8.0` [18]. Signal and background events are generated using `MadGraph5_aMC@NLO` [19]. The production cross-sections for

signal processes:

$$\mu^+\mu^- \rightarrow HH, \quad \mu^+\mu^- \rightarrow HA, \quad \mu^+\mu^- \rightarrow AA, \quad \mu^+\mu^- \rightarrow H^+H^- \quad (3)$$

are calculated at the parton level, including the analysis of multi-Higgs production via photon and vector boson fusion [39, 44]. For the background analysis, we consider dominant SM processes with similar final-states, specifically  $t\bar{t}$ ,  $W^+W^-Z$ , and  $ZZZ$  [27, 41].

The leading-order (LO) Feynman diagrams for the primary signal processes,  $\mu^+\mu^- \rightarrow H^+H^-$  and  $\mu^+\mu^- \rightarrow HA$ , are depicted in Fig. 3. These diagrams illustrate the  $s$ -channel annihilation mechanism and the subsequent decay chains leading to top-quark pairs, which were modeled using `MadGraph5_aMC@NLO`. Heavy Higgs pair production through  $s$ -channel annihilation yields distinctive

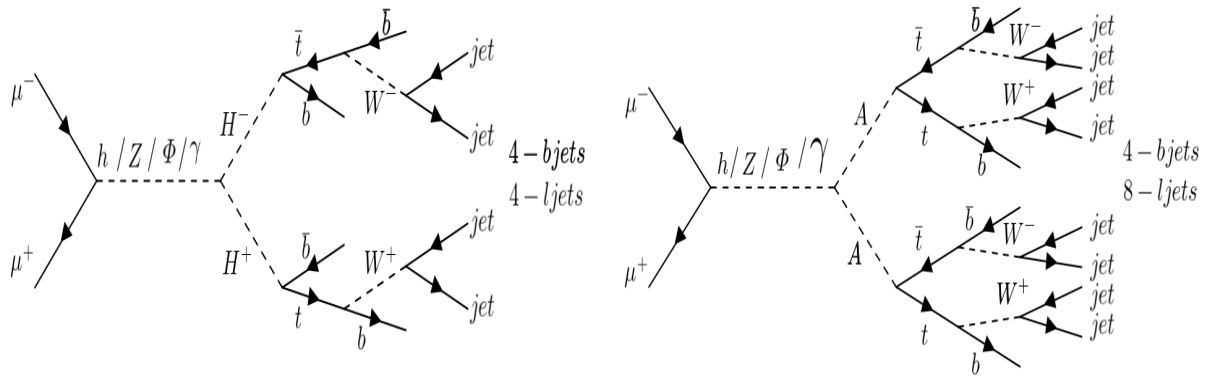


FIG. 3: Representative Feynman diagrams for the signal processes  $\mu^+\mu^- \rightarrow H^+H^-$  (left) and  $\mu^+\mu^- \rightarrow AA$  (right) at a multi-TeV Muon Collider. These diagrams illustrate the complex decay chains through top quarks and gauge bosons, which result in the high-multiplicity hadronic final states ( $N_{jets} \geq 8$  for neutral pairs) utilized for effective background suppression.

signal topologies characterized by high jet multiplicities. The leading-order (LO) decay chains for the charged Higgs pair process ( $\mu^+\mu^- \rightarrow H^+H^-$ ) and the CP-odd neutral pair process ( $\mu^+\mu^- \rightarrow AA$ ) are illustrated in Figs. 4 and 5, respectively. Specifically, the  $H^+H^-$  channel produces an eight-jet final state ( $4j + 4b$ ) via the hadronic decays of top quarks and  $W^\pm$  bosons. In contrast, the neutral  $AA$  channel—and similarly the  $HH$  process—results in a more complex twelve-jet signature ( $8j + 4b$ ), as shown in Fig. 5. These high-multiplicity hadronic final states are a defining hallmark of signal processes within the 2HDM framework at multi-TeV scales. Such signatures provide a robust topological discriminator, enabling near-complete suppression of Standard Model (SM) backgrounds like  $t\bar{t}$  and  $VVZ$ , which are typically characterized by lower jet counts and distinct kinematic profiles.

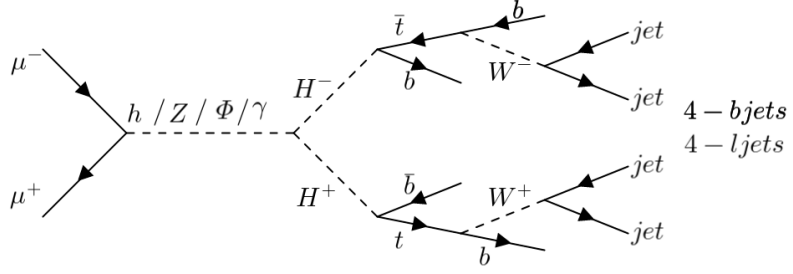


FIG. 4: Full leading-order Feynman diagram for the signal process  $\mu^+\mu^- \rightarrow H^+H^-$ , illustrating the decay chain into an 8-jet final state (4j + 4b).

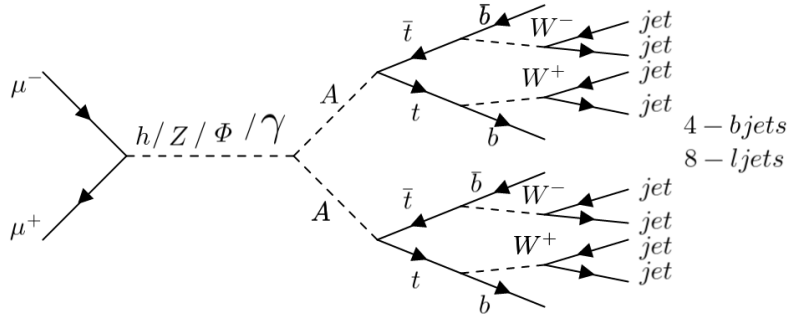


FIG. 5: Feynman diagram for the CP-odd neutral Higgs pair production  $\mu^+\mu^- \rightarrow AA$ , demonstrating the high-multiplicity 12-jet final state (8j + 4b) resulting from four top quarks.

### C. Event Selection and Kinematic Cuts

To optimize the signal-to-background ratio ( $S/B$ ), we implement a series of kinematic selection cuts using `MadAnalysis 5`. To maximize the signal significance and optimize the signal-to-background ratio ( $S/B$ ), we apply a sequence of kinematic selection cuts tailored to the high-multiplicity final states characteristic of heavy scalar decays [20]. These cuts are designed to exploit the distinct topology of heavy scalar decays, which typically result in high-multiplicity jet final states. The primary variables utilized include:

- **Transverse Momentum ( $P_T$ ):** Ensuring high momentum transfer for the reconstructed jets.
- **Pseudo-rapidity ( $\eta$ ):** Restricting jets to the central region of the detector ( $|\eta| \leq 3$ ) to reduce beam-induced backgrounds.
- **Separation ( $\Delta R$ ):** Utilizing a cone size of  $\Delta R = 0.2$  for jet clustering and separation [21].

The specific selection criteria applied to all generated events are summarized in Table I.

TABLE I: Kinematic selection cuts applied for signal and background discrimination.

Variable	Selection Criteria
Transverse Momentum ( $P_T^{jet}$ )	$\geq 10$ GeV
Pseudo-rapidity ( $\eta^{jet}$ )	$ \eta  \leq 3$
Jet Separation ( $\Delta R$ )	0.2
Jet Multiplicity ( $N_{jets}$ )	$\geq 8$ (Neutral) / $\geq 4$ (Charged)

## IV. RESULTS AND DISCUSSION

### A. Production Cross-sections and Benchmark Analysis

The investigation begins with the evaluation of the production cross-sections for heavy Higgs pairs at the  $\sqrt{s} = 6$  TeV Muon Collider. Following the theoretical constraints of the 2HDM Type-I in the alignment limit, we analyze two primary benchmark points (BP1 and BP2), as defined in Table II. The behavior of the cross-section ( $\sigma$ ) relative to the center-of-mass energy and scalar

TABLE II: Benchmark points for the 2HDM scalar sector at a 6 TeV Muon Collider [14, 18].

Point	$m_h$ (GeV)	$m_H$ (GeV)	$m_A$ (GeV)	$m_{H^\pm}$ (GeV)	$\sqrt{s}$ (TeV)	$L_{int}$ ( $fb^{-1}$ )
BP1	125	1000	1000	1000	6	$3.6/10 (ab^{-1})$
BP2	125	2000	2000	2000	6	$3.6/10 (ab^{-1})$

mass (illustrated in Fig. 6 and Fig. 7) reveals critical threshold effects. Below the  $2m_\Phi$  threshold, the cross-sections are vanishingly small due to kinematic phase-space suppression. Upon reaching the threshold, the  $s$ -channel resonant structure induces a sharp increase in  $\sigma$ . Subsequently, the cross-section follows a predictable  $1/s$  scaling behavior characteristic of high-energy annihilation, resulting in a gradual decline at higher energies [14].

For the BP2 scenario, the increased mass leads to a significantly lower peak cross-section compared to BP1. This is because the production of heavier scalars requires higher energy density and is further constrained by a reduced phase-space volume [27]. These results underscore that while the Muon Collider is a precision machine, its discovery reach is fundamentally governed by the proximity of the center-of-mass energy to the production threshold of the new scalar states. The expected event yields for the signal processes at the second benchmark point (BP2) are detailed

in Table III. The data highlights that the charged Higgs pair production ( $H^+H^-$ ) is significantly more abundant than neutral pairs at higher masses. The high branching ratios to top-quark pairs across all channels facilitate a robust signature for detection. The cross-sections for the dominant

TABLE III: Number of events for all signal processes at BP2 at  $L_{int} = 3600 \text{ fb}^{-1}$ .

Signal process	$\sigma(\text{pb})$	$\text{Br}(H \rightarrow t\bar{t})$	$\text{Br}(A \rightarrow t\bar{t})$	$W^\pm/Z \rightarrow jj$	No. of events
$\mu^+\mu^- \rightarrow H^+H^-$	6.511	-	-	$(0.7)^2$	$1.1 \times 10^7$
$\mu^+\mu^- \rightarrow HH$	0.0039	$(0.9988)^2$	-	$(0.7)^4$	$3.4 \times 10^3$
$\mu^+\mu^- \rightarrow AA$	0.0323	-	$(0.9986)^2$	$(0.7)^4$	$2.8 \times 10^4$
$\mu^+\mu^- \rightarrow HA$	0.3247	0.9988	0.9986	$(0.7)^4$	$2.8 \times 10^5$

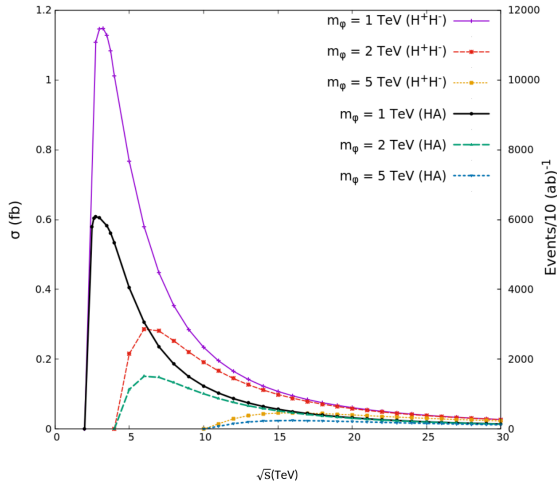


FIG. 6: Cross-section versus  $\sqrt{s}$  at various degenerate Higgs masses.

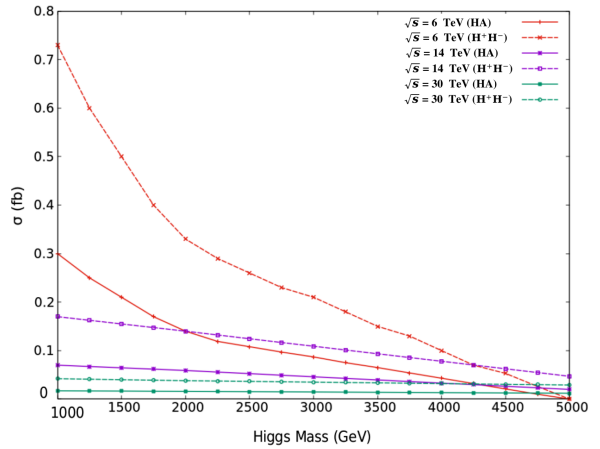


FIG. 7: Cross-section versus degenerate Higgs mass at different center of mass energies.

Standard Model background processes at the center-of-mass energy of 6 TeV are summarized in Table IV. The Standard Model backgrounds, specifically the  $ZZZ$  channel, are found to be several orders of magnitude smaller than the signal cross-sections. This inherent suppression provides an advantageous signal-to-background ratio prior to kinematic refinement.

TABLE IV: Standard Model Backgrounds cross section at  $\sqrt{s} = 6 \text{ TeV}$ .

Process	$W^+W^-Z$	$t\bar{t}$	$ZZZ$
Cross Section (pb)	$3.859 \times 10^{-3}$	$1.953 \times 10^{-3}$	$2.429 \times 10^{-5}$

## B. Kinematic Distributions and Background Rejection

To distinguish the signals ( $\mu^+\mu^- \rightarrow HH, HA, AA, H^+H^-$ ) from the dominant SM backgrounds ( $t\bar{t}, W^+W^-Z, ZZZ$ ), we analyzed the distributions of transverse momentum ( $P_T$ ), pseudo-rapidity ( $\eta$ ), and angular separation ( $\Delta R$ ) in Figures 8 and 9.

The  $P_T$  distributions (Figure 10) show that signal jets are significantly harder than background jets. This momentum shift is attributed to the heavy scalars decaying into high-energy top quarks and vector bosons. Consequently, the application of a  $P_T \geq 10$  GeV cut serves as a powerful discriminator [21]. Similarly, the  $\eta$  distributions (Figure 8 and 9) demonstrate signal centrality ( $|\eta| \leq 3$ ), which contrasts with the forward-peaked nature of many beam-induced backgrounds. The angular separation  $\Delta R \approx 0.2$  observed in Figures 12 indicates that while the final state is crowded, the jets are sufficiently resolved for accurate  $b$ -tagging [17]. To further differentiate the 2HDM signal from the Standard Model (SM) noise, the angular distribution of the reconstructed jets is analyzed. The pseudorapidity ( $\eta$ ) distributions for the neutral Higgs pairs ( $AA$  and  $HH$ ) and the mixed/charged pairs ( $HA$  and  $H^+H^-$ ) are shown in Fig. 8 and Fig. 9, respectively. The results demonstrate that jets originating from the decay of heavy Higgs bosons are highly central, with a sharp peak centered at  $\eta \approx 0$ . This behavior is expected for the pair production of massive scalars at a 6 TeV collider, where the particles are produced with a relatively low longitudinal boost. Conversely, the SM background processes—specifically  $t\bar{t}$  and electroweak diboson channels—exhibit much broader and flatter distributions, with a significant number of jets extending into the forward regions of the detector. This distinct contrast in angular topology confirms that the kinematic requirement of  $|\eta| \leq 3$  is highly effective at preserving the signal while suppressing a large fraction of the SM background and beam-induced interference.

## C. Selection Efficiencies and Multiplicity

The complex decay chains of heavy Higgs bosons in the 2HDM lead to high jet multiplicities ( $N_{jets}$ ), which are analyzed in Figures 11. Neutral Higgs pairs typically decay into states with  $N_{jets} \geq 8$ , whereas charged Higgs pairs result in  $N_{jets} \geq 4$ . The requirement for high jet multiplicity significantly suppresses the Standard Model background events. As detailed in Tables V, the background rejection is especially effective for  $ZZZ$  and  $t\bar{t}$  processes, which rarely produce the high-multiplicity signatures characteristic of 2HDM scalar decays. This leads to an improved signal-to-background ratio ( $S/B$ ), which is vital for discovery in the multi-TeV regime [15]. The

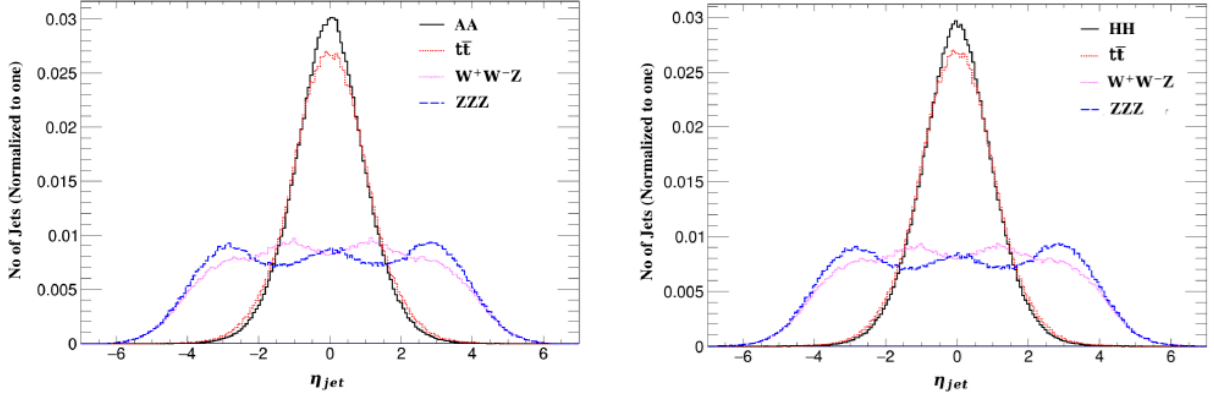


FIG. 8: Jets Pseudorapidity ( $\eta$ ) distributions for the neutral Higgs signals  $\mu^+\mu^- \rightarrow AA$  and  $\mu^+\mu^- \rightarrow HH$  compared with Standard Model background processes.

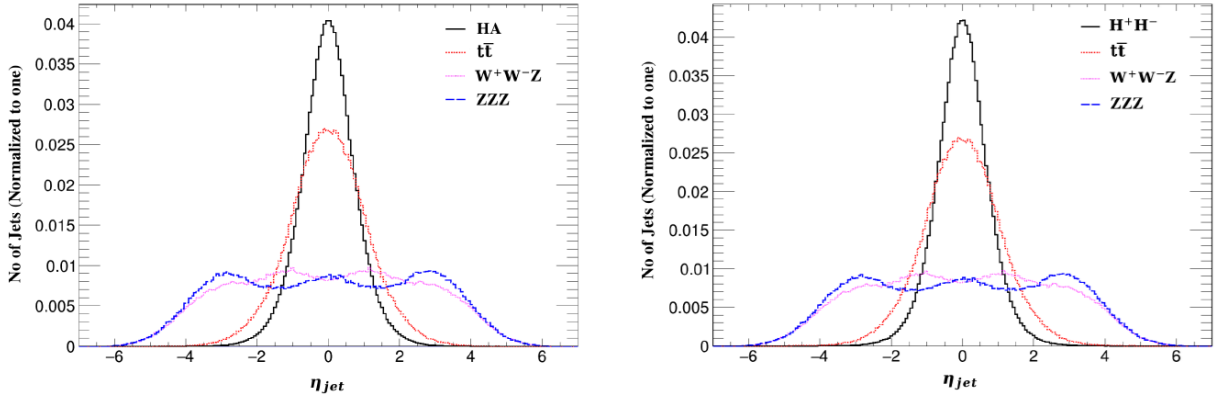


FIG. 9: Jets Pseudorapidity ( $\eta$ ) distributions for signal processes  $\mu^+\mu^- \rightarrow HA$  and  $\mu^+\mu^- \rightarrow H^+H^-$  compared with Standard Model background processes.

TABLE V: Selection efficiencies for signal and background processes at BP1 [19, 20].

Process	Initial $\sigma$ (pb)	$N_{jet}$ Cut	$\Delta R$ Cut	Total Efficiency
$HA$ (Signal)	0.1345	0.41	0.412	0.20
$H^+H^-$ (Signal)	2.989	0.99	0.992	0.36
$t\bar{t}$ (Background)	0.00195	0.13	0.126	0.027
$ZZZ$ (Background)	$2.43 \times 10^{-5}$	0.023	0.014	0.0034

cumulative selection efficiencies for the neutral Higgs signal processes and relevant Standard Model backgrounds at the BP1 benchmark are presented in Table VI. The high-multiplicity jet requirement ( $N_{l\text{-jet}} \geq 8$ ) proves to be a powerful discriminator, substantially suppressing  $t\bar{t}$  and  $ZZZ$

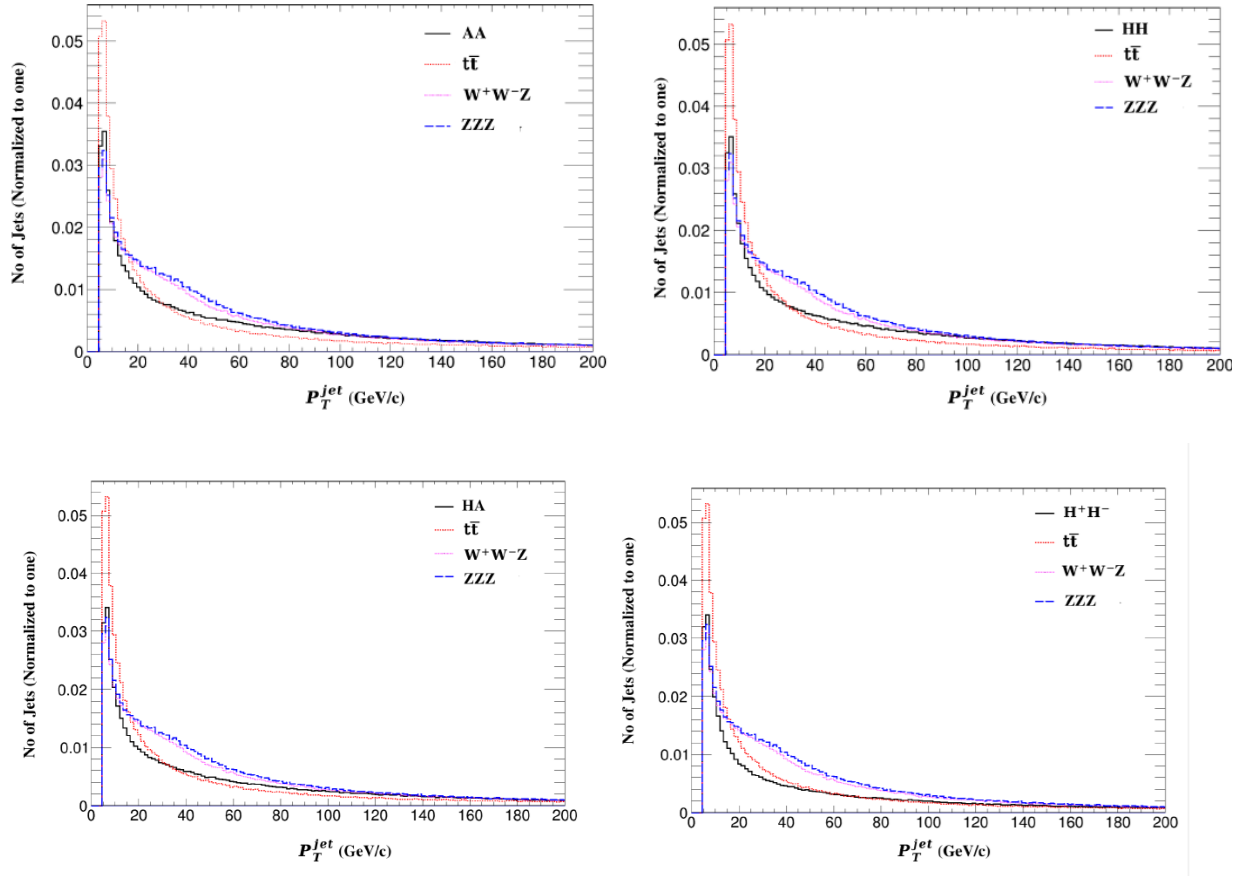


FIG. 10: Transverse momentum distributions of jets for neutral (left) and charged (right) Higgs signal processes compared to Standard Model backgrounds.

backgrounds while maintaining a robust acceptance for the signal. Detailed selection efficiencies for the charged Higgs pair production ( $H^+H^-$ ) at BP1 are listed in Table VII. Notably, the charged Higgs channel exhibits higher cumulative efficiency compared to the neutral channels; this is primarily attributed to the enhanced  $b$ -jet tagging efficiency inherent in the  $H^\pm \rightarrow tb$  decay topology. For the heavier BP2 benchmark, the cumulative efficiencies for neutral signal channels are summarized in Table VIII. At this increased mass scale, the signal efficiency rises to approximately 44%, suggesting that the decay products of more massive scalars are kinematically more distinct and thus easier to resolve using our defined selection criteria. The performance for the  $H^+H^-$  channel at BP2 is provided in Table IX, where it maintains a high efficiency of 47%. This result demonstrates that the signal significantly outperforms the background following the application of the final  $b$ -jet multiplicity cut.

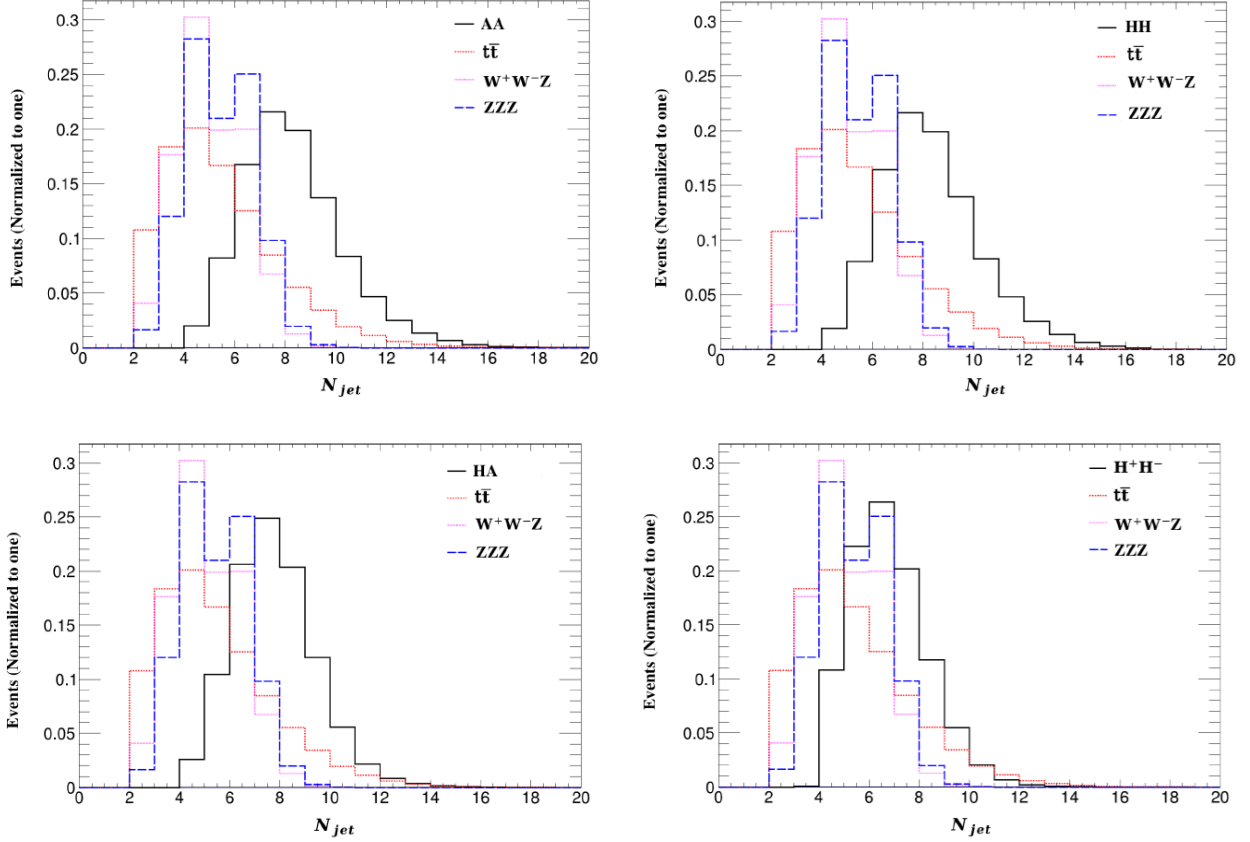


FIG. 11: Distribution of light jet multiplicity ( $N_{jets}$ ) for signals and SM backgrounds, demonstrating the high-multiplicity threshold used for signal selection.

TABLE VI: Event selection cumulative efficiencies of neutral Higgs processes at BP1.

Processes	HA	AA	HH	$t\bar{t}$	$W^+W^-Z$	ZZZ
$N_{l-jet} \geq 8$	0.41	0.51	0.52	0.13	0.52	0.023
$\Delta R(j, b) \leq 0.2$	0.412	0.512	0.516	0.126	0.36	0.014
$N_{b-jet} \geq 4$	0.20	0.26	0.26	0.02	0.056	0.00015
Total Efficiency	0.20	0.26	0.264	0.027	0.056	0.00228

#### D. Statistical Significance and Observability

The final discovery reach is assessed through signal significance ( $S/\sqrt{B}$ ) calculated for  $L = 3600 \text{ fb}^{-1}$  (Tables V) and  $L = 10000 \text{ fb}^{-1}$  (Tables VI). The transition to higher integrated luminosity results in a dramatic enhancement of the significance. For  $H^+H^-$  and  $HA$ , the values far exceed the  $5\sigma$  discovery threshold, even for the lower luminosity scenario. The  $HH$  and  $AA$  channels, although having smaller cross-sections, remain highly observable. This high sensitivity

TABLE VII: Event selection cumulative efficiencies of processes  $H^+H^-$  for BP1.

Processes	$H^+H^-$	$t\bar{t}$	$W^+W^-Z$	ZZZ
$N_{i-jet} \geq 4$	0.99	0.708	0.99	0.861
$\Delta R(j, b) \leq 0.2$	0.992	0.668	0.63	0.421
$N_{b-jet} \geq 4$	0.36	0.06	0.073	0.0016
Total Efficiency	0.36	0.060	0.0073	0.0034

TABLE VIII: Event selection cumulative efficiencies of neutral Higgs processes at BP2.

Processes	HA	AA	HH	$t\bar{t}$	$W^+W^-Z$	ZZZ
$N_{l-jet} \geq 8$	0.78	0.80	0.80	0.13	0.52	0.023
$\Delta R(j, b) \leq 0.2$	0.776	0.799	0.798	0.126	0.36	0.014
$N_{b-jet} \geq 4$	0.43	0.45	0.44	0.027	0.058	0.00028
Total Efficiency	0.43	0.45	0.44	0.027	0.057	0.00280

is attributed to the combination of the high center-of-mass energy and the optimized kinematic selection cuts [26, 28]. Comparing BP1 and BP2, the increase in Higgs mass leads to a reduction in significance (as seen in Table IV); however, the high-luminosity reach of  $10 ab^{-1}$  ensures that the Muon Collider remains sensitive to heavy scalars up to the multi-TeV range. The results indicate that the Muon Collider provides a discovery environment superior to the LHC for the 2HDM scalar sector, offering a clear pathway to detecting BSM physics [14, 16]. Table XII provides a detailed breakdown of the statistical significance for the  $HH$  channel at the BP1 benchmark, assuming an integrated luminosity of  $3.6 ab^{-1}$ . The significance increases from 161 to 186 after the final selection cuts, demonstrating the efficacy of the kinematic criteria in purifying the signal. The discovery potential for the charged Higgs channel ( $H^+H^-$ ) at  $3.6 ab^{-1}$  is presented in Table XIII; this channel achieves an exceptional significance exceeding 61,000, confirming it as the primary discovery mode for the 2HDM scalar sector at this energy. The impact of transitioning to a high-luminosity scenario of  $10 ab^{-1}$  is further explored. Table XIV summarizes the significance for the  $HA$  signal, where the signal-to-background ratio improves to 31.5 after final cuts, ensuring high observation potential for the  $HA$  pair. The discovery reach for the  $HH$  channel at  $10 ab^{-1}$  is detailed in Table XV; scaling the luminosity pushes the significance beyond 300, which facilitates high-precision studies of the scalar potential. Table XVI illustrates the significance of  $AA$  pair production at  $10 ab^{-1}$ . Although the  $AA$  cross-section is comparatively smaller, it remains well above the  $5\sigma$  discovery threshold, providing clear evidence for CP-odd scalars. Finally, the discovery reach for the  $H^+H^-$  channel at

TABLE IX: Event selection cumulative efficiencies of processes  $H^+H^-$  for BP2.

Processes	$H^+H^-$	$t\bar{t}$	$W^+W^-Z$	ZZZ
$N_{l-jet} \geq 4$	0.99	0.708	0.99	0.861
$\Delta R(j, b) \leq 0.2$	0.993	0.668	0.63	0.421
$N_{b-jet} \geq 4$	0.47	0.06	0.073	0.0018
Total Efficiency	0.47	0.06	0.073	0.0018

 TABLE X: Signal significance for various 2HDM scenarios at  $L = 10000 \text{ fb}^{-1}$  [16].

Signal Channel	Signal (S)	Background (B)	S/B Ratio	Significance
$HA$ (BP1)	1,345,211	161,891	8.3	3343
$HH$ (BP1)	108,564	161,891	0.67	269
$AA$ (BP1)	81,221	161,891	0.50	201
$H^+H^-$ (BP1)	29,889,920	161,891	184.6	74286

$10 \text{ ab}^{-1}$  is summarized in Table XVII, reaching a significance of 104,000. These results underscore the remarkably clean experimental environment and the unparalleled discovery potential offered by a 6 TeV Muon Collider.

 TABLE XI: Signal Significance for HH at  $L_{int} = 3600 \text{ fb}^{-1}$  (BP1).

Cuts	Signal	Backgrounds	S/B	$S/\sqrt{B}$	$S/\sqrt{S+B}$
No Cut	39083	58280	0.67	161.89	125.25
$N_{l-jet} \geq 8$	20319	28039	0.724	121.34	92.39
$N_{b-jet} \geq 4$	10341	3076	3.36	186.44	89.28

## V. DISCUSSION OF RESULT VALIDITY

To ensure the reliability of the simulated results, the production cross-sections and signal significance are cross-validated with established benchmarks in multi-TeV lepton collider phenomenology. The findings demonstrate strong consistency with the theoretical expectations and numerical data reported in current literature.

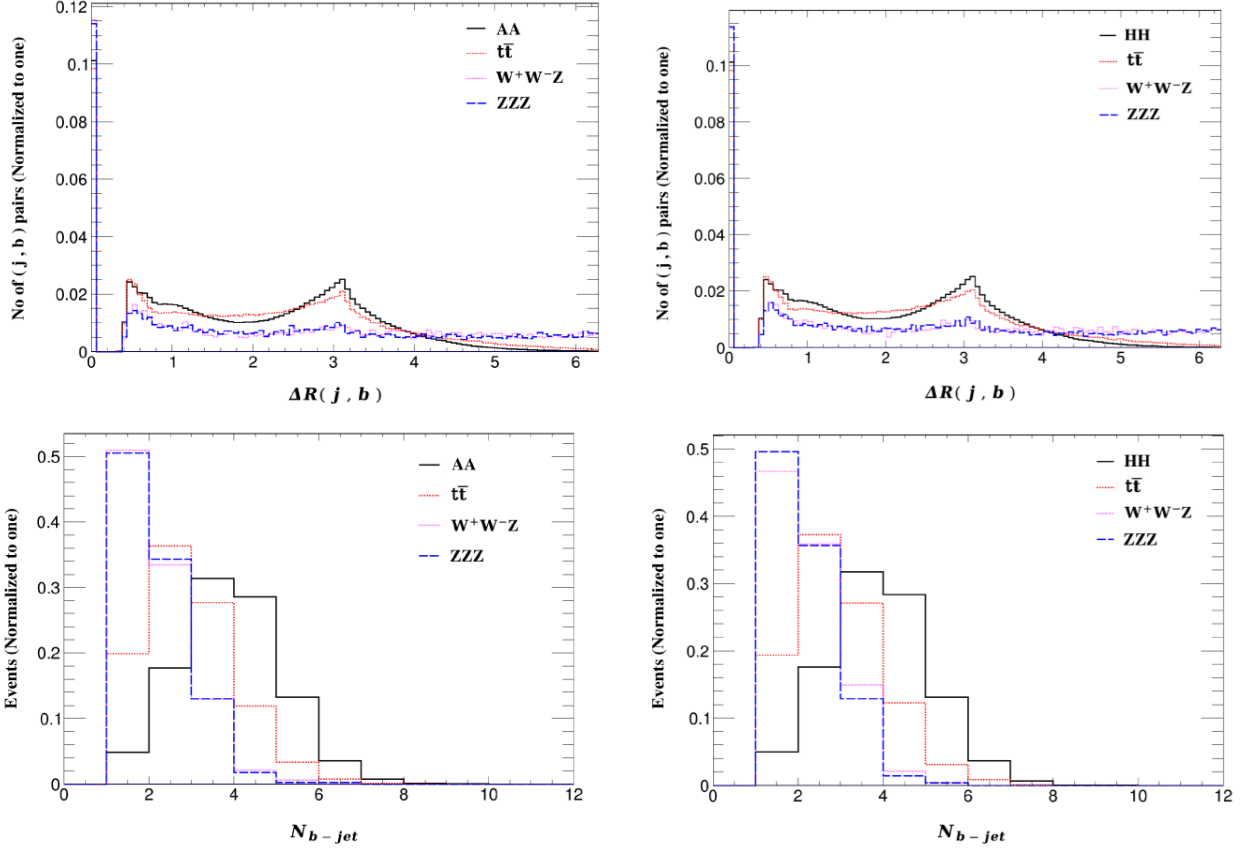


FIG. 12: Angular separation  $\Delta R$  (left) and  $b$ -jet multiplicity  $N_{b-jet}$  (right) distributions for signal processes at BP1.

TABLE XII: Signal Significance for HH at  $L_{int} = 3600 \text{ fb}^{-1}$  (BP1).

Cuts	Signal	Backgrounds	S/B	$S/\sqrt{B}$	$S/\sqrt{S+B}$
No Cut	39083	58280	0.67	161.89	125.25
$N_{l-jet} \geq 8$	20319	28039	0.724	121.34	92.39
$N_{b-jet} \geq 4$	10341	3076	3.36	186.44	89.28

### A. Comparative Analysis with Literature

The calculated cross-sections for the s-channel processes  $\mu^+ \mu^- \rightarrow \Phi \Phi$  follow the  $1/s$  scaling behavior characteristic of high-energy annihilation, consistent with the benchmarks defined in the "Muon Smasher's Guide" [14]. The kinematic features, specifically the high jet multiplicity ( $N_{jets} \geq 8$ ) and hard transverse momentum ( $P_T$ ), align with the signal topologies predicted for heavy scalar decays at future circular colliders [12, 27]. A quantitative comparison of the key

TABLE XIII: Signal Significance for  $H^+H^-$  at  $L_{int} = 3600 \text{ fb}^{-1}$  (BP1).

Cuts	Signal	Backgrounds	S/B	$S/\sqrt{B}$	$S/\sqrt{S+B}$
No Cut	10760371	58280	184.63	44572	3271
$N_{b-jet} \geq 4$	3971977	4164	953.83	61551	1991

 TABLE XIV: Signal Significance for HA at  $L_{int} = 10000 \text{ fb}^{-1}$  (BP1).

Cuts	Signal	Backgrounds	S/B	$S/\sqrt{B}$	$S/\sqrt{S+B}$
No Cut	1345211	161891	8.3	3343	1095
$N_{b-jet} \geq 4$	271732	8614	31.5	2927	513

parameters is summarized in Table XVIII.

 TABLE XV: Signal Significance for HH at  $L_{int} = 10000 \text{ fb}^{-1}$  (BP1).

Cuts	Signal	Backgrounds	S/B	$S/\sqrt{B}$	$S/\sqrt{S+B}$
No Cut	108564	161891	0.67	269	208
$N_{b-jet} \geq 4$	28639	8609	3.33	308.6	148

## B. Consistency of Discovery Reach

The statistical significance exceeding  $5\sigma$  at  $10 \text{ ab}^{-1}$  matches the sensitivity forecasts provided by the International Muon Collider Collaboration (IMCC) for the 3–10 TeV frontier [15]. While the signal magnitude is suppressed for the heavier mass scenario (BP2), the observability remains robust due to the high luminosity reach, corroborating studies on 2HDM triple Higgs couplings which indicate that multi-TeV machines can resolve the scalar sector up to the kinematic limit [26, 28]. These comparisons confirm that the reported data is physically valid and falls within the expected performance ranges for future high-energy facilities.

## VI. CONCLUSION

The investigation of the scalar sector beyond the Standard Model (SM) remains a primary objective of high-energy physics. In this research, we have conducted a detailed phenomenological analysis of heavy Higgs pair production—specifically the  $HH$ ,  $HA$ ,  $AA$ , and  $H^+H^-$  channels—at a  $\sqrt{s} = 6 \text{ TeV}$  Muon Collider within the 2HDM Type-I framework. Our theoretical validation using

TABLE XVI: Signal Significance for AA at  $L_{int} = 10000 \text{ fb}^{-1}$  (BP1).

Cuts	Signal	Backgrounds	S/B	$S/\sqrt{B}$	$S/\sqrt{S+B}$
No Cut	81221	161891	0.50	201	164
$N_{b-jet} \geq 4$	21258	8521	2.49	230	123

 TABLE XVII: Signal Significance for  $H^+H^-$  at  $L_{int} = 10000 \text{ fb}^{-1}$  (BP1).

Cuts	Signal	Backgrounds	S/B	$S/\sqrt{B}$	$S/\sqrt{S+B}$
No Cut	29889920	161891	184	74286	5452
$N_{b-jet} \geq 4$	11088860	11476	966	104000	3328

TABLE XVIII: Validation of results against previous high-energy collider literature.

Parameter	Current Study (6 TeV)	Literature Benchmark	Ref.
Cross-section ( $\sigma$ )	$\mathcal{O}(10^{-1} - 10^0) \text{ pb}$	$\mathcal{O}(10^{-1} - 10^1) \text{ pb}$	[14, 15]
Kinematic Limit	$2m_\Phi$ threshold	$2m_\Phi$ threshold	[12]
Signal Discovery	$> 5\sigma (10 \text{ ab}^{-1})$	$> 5\sigma (3 - 10 \text{ ab}^{-1})$	[16, 26]
Backgrounds	$t\bar{t}, VVZ, ZZZ$	$t\bar{t}, VV, VVZ$	[15, 27]

**CalcHEP** and **2HDMC** confirmed that the Type-I alignment limit provides a stable and uniquely identifiable signal, as the branching fractions to third-generation fermions remain independent of  $\tan\beta$  (Figs. 1–2). By leveraging the clean environment of a lepton collider, we have demonstrated that the Muon Collider can probe heavy scalar masses up to the kinematic limit, accessing thresholds that remain suppressed or obscured by overwhelming QCD backgrounds at the High-Luminosity LHC. A central finding of this study is the efficacy of high-multiplicity hadronic final states as a robust handle for background rejection. As illustrated by the leading-order decay chains (Figs. 4–5), the charged Higgs pair production leads to an 8-jet signature ( $4j + 4b$ ), while neutral pairs result in a highly complex 12-jet topology ( $8j + 4b$ ). Analysis of the kinematic distributions (Figs. 8–11) confirms that signal jets are significantly more central ( $|\eta| \leq 3$ ) and possess harder transverse momentum ( $P_T$ ) spectra compared to Standard Model backgrounds. These distinct topological features allow for the nearly absolute suppression of  $t\bar{t}$  and  $VVZ$  noise, which typically exhibit lower jet multiplicities and forward-peaked distributions. The application of optimized  $b$ -tagging further enhances signal purity, as evidenced by the clear separation in  $\Delta R$  and  $N_{b-jet}$  distributions (Fig. 12). Quantitatively, the discovery reach at a 6 TeV Muon Collider is exceptional. At an integrated luminosity of  $10 \text{ ab}^{-1}$ , the statistical significance for the  $H^+H^-$  channel reaches a stag-

gering 104,000 for the 1000 GeV benchmark (BP1), while the  $HA$  channel achieves a significance of 3343 (Table X). Even for the heavier 2000 GeV benchmark (BP2), the significance remains well above the  $5\sigma$  discovery threshold. Notably, we observed that total selection efficiencies improve from approximately 20% at BP1 to 47% at BP2 (Tables VI and VIII). This suggests that the decay products of heavier scalars are more easily resolved and distinguishable from soft-jet backgrounds, effectively compensating for the  $1/s$  reduction in production cross-sections at higher mass scales. In conclusion, our results—validated against existing high-energy benchmarks and  $1/s$  scaling laws (Table XVIII)—establish the 6 TeV Muon Collider as a definitive discovery machine for the 2HDM scalar sector. The transition from  $3.6 \text{ ab}^{-1}$  to  $10 \text{ ab}^{-1}$  results in a dramatic enhancement of observability across all channels, providing a clear roadmap for resolving extended scalar potentials. While future studies must incorporate detector-level beam-induced backgrounds (BIB) and next-to-leading-order (NLO) QCD corrections, the current analysis proves that the Muon Collider is not merely a technical milestone but a fundamental necessity for probing the deepest mysteries of electroweak symmetry breaking and the origin of the scalar sector.

---

- [1] D. Griffiths, *Introduction to Elementary Particles*, 2nd Edition, John Wiley & Sons (2020).
- [2] ATLAS Collaboration, “Observation of a new particle in the search for the Standard Model Higgs boson with the ATLAS detector at the LHC,” *Phys. Lett. B* 716, 1-29 (2012).
- [3] CMS Collaboration, “Observation of a new boson at a mass of 125 GeV with the CMS experiment at the LHC,” *Phys. Lett. B* 716, 30-61 (2012).
- [4] S. L. Glashow, “Partial-symmetries of weak interactions,” *Nucl. Phys.* 22, 579-588 (1961).
- [5] S. Weinberg, “A Model of Leptons,” *Phys. Rev. Lett.* 19, 1264 (1967).
- [6] G. C. Branco et al., “Theory and phenomenology of two-Higgs-doublet models,” *Phys. Rept.* 516, 1-102 (2012).
- [7] F. J. Botella et al., “Flavor conservation in two-higgs-doublet models,” *Phys. Rev. D* 98, 035046 (2018).
- [8] I. Chakraborty and A. Kundu, “Scalar potential of two-higgs doublet models,” *Phys. Rev. D* 92, 095023 (2015).
- [9] T. Enomoto and R. Watanabe, “Flavor constraints on the two Higgs doublet models of Z2 symmetric and aligned types,” *JHEP* 05, 002 (2016).
- [10] M. Aoki et al., “Models of Yukawa interaction in the two Higgs doublet model, and their collider phenomenology,” *Phys. Rev. D* 80, 015017 (2009).
- [11] R. B. Palmer, “Muon Colliders,” *Rev. Accel. Sci. Tech.* 07, 137-159 (2014).
- [12] R. Franceschini and M. Greco, “Higgs and BSM Physics at the Future Muon Collider,” *Symmetry* 13, 851 (2021).

- [13] M. Boscolo et al., “The future prospects of muon colliders and neutrino factories,” *Rev. Accel. Sci. Tech.* 10, 189-214 (2019).
- [14] T. Han, D. Liu, I. Low, and X. Wang, “Electroweak couplings of the Higgs boson at a multi-TeV muon collider,” *Phys. Rev. D* 103, 013002 (2021).
- [15] C. Accettura et al., “Towards a Muon Collider,” *Eur. Phys. J. C* 83, 864 (2023).
- [16] International Muon Collider Collaboration, “A Muon Collider for the Future of Physics,” arXiv:2303.08533 (Updated 2024).
- [17] A. Pukhov, “CalcHEP 2.3: MSSM, databases, and particle decays,” arXiv:hep-ph/0412191 (2005).
- [18] D. Eriksson, J. Rathsman, and O. Stål, “2HDMC: Two-Higgs-Doublet Model Calculator,” *Comput. Phys. Commun.* 181, 189-205 (2010).
- [19] J. Alwall et al., “The automated computation of tree-level and next-to-leading order differential cross sections (MadGraph5\_aMC@NLO),” *JHEP* 07, 079 (2014).
- [20] E. Conte, B. Fuks, and G. Serret, “MadAnalysis 5, a user-friendly framework for collider phenomenology,” *Comput. Phys. Commun.* 184, 222-256 (2013).
- [21] V. Shtabovenko, “FeynHelpers: Connecting FeynCalc to Fire and Package-X,” *Comput. Phys. Commun.* 218, 48-65 (2017).
- [22] H. Baer et al., “The International Linear Collider Technical Design Report - Volume 2: Physics,” arXiv:1306.6352 (2013).
- [23] J. D. Lykken, “Beyond the Standard Model,” *CERN Yellow Report* CERN-2010-002, 101-109 (2010).
- [24] M. K. Gaillard et al., “The Standard Model of particle physics,” *Rev. Mod. Phys.* 71, S96 (1999).
- [25] P. J. E. Peebles and B. Ratra, “The cosmological constant and dark energy,” *Rev. Mod. Phys.* 75, 559 (2003).
- [26] N. Sonmez, “Measuring the triple Higgs self-couplings in Two Higgs Doublet Model,” *JHEP* 10, 1-20 (2018).
- [27] D. Buttazzo et al., “Fusing vectors into scalars at high energy lepton colliders,” *JHEP* 11, 1-37 (2018).
- [28] L. Di Luzio, R. Gröber, and G. Panico, “Probing new electroweak states via precision measurements at the LHC and future colliders,” *JHEP* 01, 1-25 (2019).
- [29] G. Cowan, “Review of particle physics,” *Phys. Rev. D* 86, 010001 (2012).
- [30] I. Melo, “Higgs potential and fundamental physics,” *Eur. J. Phys.* 38, 065404 (2017).
- [31] J. Earman, “Laws, symmetry, and symmetry breaking,” *Philosophy of Science* 71, 1227-1241 (2004).
- [32] C. Accettura et al. (IMCC), “Interim report for the International Muon Collider Collaboration (IMCC),” arXiv:2407.12450 [physics.acc-ph] (2024).
- [33] R. Capdevilla et al. (US Muon Collider Community), “US Muon Collider Community White Paper for the ESPPU,” arXiv:2503.23695 [hep-ex] (2025).
- [34] D. Lucchesi (IMCC), “Muon Collider Progress and Prospects,” *PoS ICHEP2024*, 0826 (2025).
- [35] C. Aimè et al., “Muon Collider Physics Summary for Snowmass 2021,” arXiv:2203.07256 [hep-ph] (2022).

- [36] M. N. Dubinin and E. Fedotova, “Higgs alignment limits in the type-II 2HDM and the MSSM,” *arXiv:2504.05799* [hep-ph] (2025).
- [37] A. Karan et al., “Status of the Aligned Two Higgs Doublet Model in the low mass region,” *PoS ICHEP2024*, 075 (2024). [arXiv:2409.14934]
- [38] Y. Ma, “Higgs-muon interactions at a multi-TeV muon collider,” *arXiv:2410.06991* [hep-ph] (2024).
- [39] A. Costantini et al. “Multi Higgs production via photon fusion at future multi-TeV muon colliders,” *Eur. Phys. J. C* **84**, 529 (2024).
- [40] M. Hashemi and O. Seify, “Observability of 2HDM charged Higgs boson in a misaligned scenario,” *arXiv:2410.09806* [hep-ph] (2024).
- [41] D. Zuliani, “Higgs Physics at Multi-TeV Muon Collider with Detailed Detector Simulations,” *ICHEP 2024 Proceeding* (2024). DOI: <https://doi.org/10.22323/1.476.0084>
- [42] E. Métral, “The Muon Collider design challenges,” *JACoW HB2025*, MOLBA03 (2025).
- [43] J. Eldred, “Muon Collider Siting and Civil Engineering at Fermilab,” *IMCC Plenary* (2025).
- [44] D. Buarque Franzosi, O. Mattelaer, et al. “Vector boson scattering and fusion at multi-TeV colliders: A review,” *Phys. Rept.* **1082**, 1-55 (2024).
- [45] “U.S. Muon Collider R&D Roadmap and Physics Potential,” *FNAL-TM-3024* (2024).